Confinement-Induced Reduction in Phase Segregation and Interchain Disorder in Bulk Heterojunction Films

Ahsan Ashraf,[†,‡] D. M. Nanditha M. Dissanayake,[‡] David S. Germack,[§] Conan Weiland,[⊥] and Matthew D. Eisaman[†,‡,*]

[†]Department of Physics and Astronomy, Stony Brook University, Stony Brook, New York 11974, United States, [‡]Sustainable Energy Technologies Department, Brookhaven National Laboratory, Upton, New York 11973, United States, [§]Condensed Matter Physics and Materials Science Department, Brookhaven National Laboratory, Upton, New York 11973, United States, and [⊥]Synchrotron Research, Inc., Upton, New York 11973, United States

ABSTRACT The effects of thin-film confinement on the material properties of ultrathin polymer (electron donor):fullerene (electron acceptor) bulk heterojunction films can be important for both fundamental understanding and device applications such as thin-film photovoltaics. We use variable angle spectroscopic ellipsometry and near edge X-ray absorption fine structure spectroscopy to measure the optical constants, donor—acceptor volume fraction profile, and the degree of interchain order as a function of the thickness of a poly(3-hexythiophene-2,5-diyl) and phenyl-C61-butyric acid methyl ester bulk heterojunction film. We find that as the thickness of the bulk heterojunction film is decreased from 200 nm to the thickness confinement regime (less than 20 nm), the vertical phase segregation gradient of the donor and acceptor phases becomes less pronounced. In addition, observing the change in exciton bandwidth and the shift of absorption resonances (0—0 and 0—1) relative to neat donor and acceptor films, we find that the conjugation length and disorder in ultrathin films (20 nm) are less affected than thicker (200 nm) films by the addition of fullerene into the polymer. We believe that these findings could be important for discovering methods of precisely controlling the properties of bulk heterojunction films with crucial implications for designing more efficient organic-based photovoltaics.

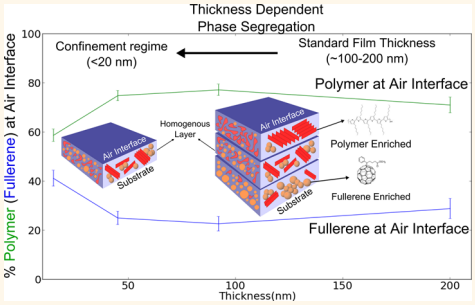

KEYWORDS: phase segregation · confinement · spectroscopic ellipsometry · polymer:fullerene bulk heterojunction · organic photovoltaics · thin films

Restriction of the film thickness below the radius of gyration in macromolecules leads to thin-film confinement effects, in which a significant transition of the materials properties occurs compared to bulk films.[1−4] Even though thin-film confinement is well studied for both amorphous and crystalline pure polymers,[5] its effects on the morphology and the interfacial interactions of ultrathin (<20 nm, the length scales comparable to the polymers radius of gyration)[6] polymer (electron donor):fullerene (electron acceptor) interpenetrating composites, bulk heterojunction (BHJ) films, have not been well investigated.[7] BHJs are a more complex and functionally more advanced class of composite materials, and a fundamental understanding of the effect of thin-film confinement on BHJ films could be crucial for applications such as novel organic photovoltaics. In BHJ films, even within a bulk thickness regime of ~200 nm, its morphology is reported to be affected by various processing conditions such as choice of solvent, drying time, thermal treatments,[8] and the use of solvent additives.[9,10] Furthermore, depending on the surface energy of the substrate on which such BHJs are coated, an inhomogeneous distribution of the polymer:fullerene volume fraction, phase segregation, in the direction normal to the substrate has been reported.[11,12] These morphological and interfacial phenomena directly impact the optical and electronic properties of the BHJ layer critical for device applications.[8] In particular, the high- and low-bandgap polymer regions within the bulk of the BHJ layer believed to be formed by phase segregation are directly linked to the reduction in bimolecular recombination of BHJ based organic photovoltaics, and this is perceived

* Address correspondence to meisaman@bnl.gov.

Received for review August 9, 2013 and accepted December 20, 2013.

Published online December 20, 2013
10.1021/nn404172m

to be one crucial reason for its outstanding performance among solution processed thin-film photovoltaics.[13,14] Therefore, a thorough understanding of these properties (*i.e.*, morphology, phase-segregation) and their possible variation within the thin-film confinement regime are important for both a fundamental understanding of the material system, as well as for novel device applications. In particular, ultrathin active layer could improve the limitation in charge collection in BHJ, which, together with improved light-trapping to compensate the concomitant loss in optical density in ultrathin regime, would boost the overall performance in organic photovoltaics. Pang *et al.*[15] have demonstrated a novel organic photovoltaic design where the absorption fraction of a guided mode in a 20 nm thick bulk heterojunction active layer can be equal to the absorption fraction for light that is normally incident on a standard 100 nm active layer. In addition, many other groups have recently demonstrated strong optical absorption in similarly thin photoactive layers.[16−22]

In this work, we use spectroscopic ellipsometry and near edge X-ray absorption fine structure (NEXAFS) spectroscopy to measure the optical constants, vertical composition profile (donor−acceptor ratio), and morphology of poly[3-hexylthiophene-2,5-diyl] (P3HT) and [6,6]-phenyl C61 butyric acid methyl ester (PCBM) BHJ layer as a function of thickness. We find that as the thickness of the BHJ is decreased from the range of 100−200 nm to the ultrathin regime of <20 nm, surface-energy effects at the interfaces play an increasingly important role in determining the BHJ morphology and phase segregation.[12] In addition, as a function of BHJ thickness we measure the change of refractive index and shift of the dipole-transition resonance frequencies relative to neat donor and acceptor films to gain insight into the domain structure and degree of order in the interpenetrating donor−acceptor phases. The data is interpreted *via* a rigorous optical model that divides the BHJ into multiple sections in the substrate-normal direction, allowing a reconstruction of the vertical phase segregation profile (variation of P3HT/PCBM volume fraction ratio in the substrate normal direction) from spectroscopic ellipsometry (SE) data. Additionally, we validate the SE measurements by directly measuring the P3HT/PCBM ratio at the top (film−air) surface of the BHJ using NEXAFS.

Using spin-cast BHJ films (100−15 nm) onto poly-(3,4-ethylenedioxythiophene) poly(styrenesulfonate) (PEDOT-PSS) on multiple substrates (silicon, quartz, and glass), we find that the PCBM volume fraction at the PEDOT-PSS/BHJ interface increases as a function of film thickness, and the PCBM percentage at the BHJ/air interface decreases as the film thickness is increased. Using this data we believe that BHJ blend films get less phase separated as the film thickness is reduced, primarily because of thin-film confinement effects that out-compete the mechanisms of surface-energy directed interfacial enrichment. Crucially, we observe that ultrathin (<20 nm) BHJ films have nearly a single-phase (*i.e.*, very little vertical gradient in donor or acceptor volume fraction), which could affect its applicability as a high-performance photoactive layer with reference to lower bimolecular recombination and charge transport benefits seen in phase-segregated BHJ films.[23,24]

The optical modeling of these BHJ systems requires accurate measurements of the optical properties, particularly the complex refractive index, $\tilde{n} = n + ik$. The change in BHJ nanomorphology and phase segregation that occurs with varying BHJ thickness also causes changes in the complex refractive index of the BHJ layer with varying thickness, including vertical gradients in the refractive index within the BHJ film. While there have been optical studies among different polymer-fullerene blends, to date there have been no detailed studies of the change in complex refractive indices as a function of the thickness, and throughout the thickness, of a BHJ film.[12,25,26] Assuming that the phase segregation of a standard thickness (100−200 nm) active layer holds for any thickness will lead to inaccurate calculations and suboptimal designs when exploring new device architectures with varying thickness active layers.

RESULTS AND DISCUSSION

We present an analysis of SE data for P3HT:PCBM BHJ films with thicknesses ranging from 15 to 100 nm. Data were collected from films on multiple substrates to account for different surface roughnesses and to increase the number of data sets. An effective medium approximation was used for the film−substrate interface and for the film−air interface. In general, out-of-plane to in-plane optical anisotropy has been seen in P3HT:PCBM films due to the orientation of the P3HT polymer chains.[12] Any preferential molecular orientation changes in these thin films will result in a change in the complex refractive index data.[27] The data is interpreted in terms of a model that divides the BHJ into multiple sections in the substrate-normal direction, allowing a reconstruction of the vertical phase segregation profile (variation of P3HT/PCBM volume fraction ratio in the substrate-normal direction) from the SE data. We corroborate these results from SE *via* direct measurement of the P3HT/PCBM volume-fraction using NEXAFS measurements.

The analysis of the ellipsometric data was done using the J. A. Woollam software, WVASE32 (version 3.770). First, the optical constants for the pristine P3HT and PCBM films were obtained. Earlier studies have shown that P3HT films are anisotropic and PCBM films are isotropic.[28] The optical constants for the P3HT films were obtained using a uniaxial model ($\tilde{n}_x = \tilde{n}_y \neq \tilde{n}_z$, where z is the substrate-normal direction). In constructing

this model, the first step is to estimate thickness of the film with a Cauchy parametrization[29] in the wavelength region where the film is transparent (>1000 nm),

$$n(\lambda) = A + \frac{B}{\lambda^2} + \frac{C}{\lambda^4} \quad (1)$$

$$k(\lambda) = \alpha e^{\beta(12400(\frac{1}{\lambda}-\frac{1}{\gamma}))} \quad (2)$$

where n and k are the real and imaginary parts of the refractive index, and λ is the wavelength. This is a six parameter model where α is the extinction coefficient amplitude, β is the exponent factor, and γ is the band edge. The parameters were determined by a best-fit algorithm.

The thickness obtained *via* the Cauchy parametrization was verified using alternative methods such as profilometry and atomic force microscopy in tapping mode (Supporting Information), and was then used as a fixed parameter in the model. A point-by-point fit, *i.e.*, a direct extraction of n and k calculated from the directly measured SE data (typically referred to as ψ and Δ)[29] on a wavelength-by-wavelength basis, was performed over the entire wavelength range to give a preliminary estimate of the optical constants. These values for n and k were used as a reference to the parametrized model. A generalized oscillator model was used to parametrize the complex refractive index of the film. For the polymer films, we used a uniaxial layer (in order to accurately model anisotropy), with a 4-peak Lorentz oscillator in the in-plane direction and 1-peak in the out-of-plane direction. Two peaks for vibronic exciton transitions (0−0 and 0−1) at ∼2.05 and ∼2.22 eV, a peak at ∼2.43 eV for the $\pi-\pi^*$ transition and a peak at ∼1.5 eV for the delocalized polarons were used.[12,26,30] For the fullerene films, we used an isotropic model, a 3-peak Lorentz oscillator with peaks at 3.64, 4.53, and 5.74 eV, which can be asigned to PCBM electronic transitions.[31] The Lorentz oscillator was written in the form given in eq 3 and 4,

$$\varepsilon = \varepsilon_1 + i\varepsilon_2 = (n + ik)^2 \quad (3)$$

$$\varepsilon = \varepsilon_{1\infty} + \sum_j \frac{A_j}{E_j^2 - (h\nu)^2 - iB_j h\nu} \quad (4)$$

where ε is the dielectric constant, with real and imaginary parts ε_1 and ε_2, and eq 3 relates the dielectric constant to the real and imaginary parts of the refractive index. In eq 4, h is Planck's constant, ν is the optical frequency, and for a 5-peak oscillator, $j = 5$ where A_j is the amplitude, E_j is the center energy, B_j is the broadening of each oscillator, and $\varepsilon_{1\infty}$ is an additional offset term varied by the model. The software uses a complete analytical solution to the Kramers−Kronig integral.[32]

The optical constants for these films were found without any *a priori* assumptions. As opposed to PCBM, P3HT films have an absorption spectrum that is highly dependent on the processing conditions of the films.[12] However, control films (∼100 nm) were made using similar conditions to the BHJ films, and the optical constants we measured were similar to those found in literature.[12] The pure PCBM optical constants were also found be to be close to previously measured values quoted in the literature.[12,33,34]

Once the optical constants of the pristine P3HT and PCBM films were determined, we modeled the optical data from the blend films using an effective medium approximation (EMA). This was a simple linear combination of the pristine optical constants using the Bruggeman approach.[29,35,36] The resulting dielectric function ε for the mixture of two materials a and b is given by eq 5,

$$\varepsilon = \frac{\varepsilon_a\varepsilon_b + \kappa\varepsilon_h(f_a\varepsilon_a + f_b\varepsilon_b)}{\kappa\varepsilon_h + (f_a\varepsilon_a + f_b\varepsilon_b)} \quad (5)$$

where ε_a and ε_b were the complex dielectric constants of materials a and b repectively, and f_a and f_b were the volume fractions of the two materials. In the Bruggeman approach, $\kappa = 2$ and $\varepsilon_h = \varepsilon$.[29] We constructed a model where the optical constants of the pristine P3HT and PCBM were fixed, and only the volume fraction of the materials was allowed to vary.

For comparison, a different model for the BHJ blend was also constructed where the blend was considered as an independent material rather than using an EMA. In this approach, the BHJ material was modeled using a uniaxial layer (to account for anisotropy) with a 7-peak Lorentz oscillator in the in-plane direction (4 Lorentz oscillators for P3HT and 3 oscillators for PCBM) and a 1-peak Lorentz oscillator in the out-of-plane direction.

A linear concentration gradient of the fullerene in polymer/fullerene blend films in the substrate-normal direction was first shown in 2002 by Arias *et al.* using atomic force microscopy and in 2008 by Campoy-Quiles *et al.* using SE.[11,25] The linear nature of the gradient was shown to be oversimplified by Germack *et al.*[12] by using a three-layer EMA model to show that in the blend films, P3HT enriched regions form at the air/film interface and PCBM enriched regions at the substrate/film interface for high surface-energy substrates. Using neutron reflectivity, Kiel *et al.* have also shown a similar trend due to surface-energy effects of the substrate.[37]

Our ellipsometric modeling uses a three layer EMA approach for films greater than 20 nm thicknesses and a two layer EMA for thinner films. For each of the thicknesses studied, the PCBM volume fraction of the top EMA layer (with thickness of 5 nm) is constrained to be equal to the value measured using NEXAFS. The volume fraction of the other EMA layers was found by minimizing the mean squared error (MSE). For the thicker films (∼100−200 nm), our findings agree with the results of the previous studies.[12]

Once the accuracy and reliability of the ellipsometric model was tested in several ways (Supporting Information), the model was used to derive optical constants for 90, 45, and 15 nm thick BHJ films. We quantify the optical anisotropy using the anisotropy parameter $A(\lambda)$ in eq 6,[38]

$$A(\lambda) = k(\lambda)_{\text{in-plane}} - k(\lambda)_{\text{out-of-plane}} \quad (6)$$

where λ is wavelength, $k(\lambda)_{xy}$ and $k(\lambda)_z$ are the imaginary parts of the refractive index within and perpendicular to the plane of the film, and the variation in the difference between $k(\lambda)_{xy}$ and $k(\lambda)_z$ gives a measure of the anisotropy of the films. Using the multilayer EMA model described earlier, we can also quantify the phase segregation of P3HT and PCBM as a function of depth in the substrate-normal direction of the film. The optical constants and the optical anisotropy in the three regions along with the phase segregation for films of different thickness are shown in Figure 1a–c.

In all cases, the optical constants changed as a function of the thickness of the film. Closer to the substrate, the films are PCBM-rich and show optical anisotropy in the range of 0–0.25. In the top 5 nm of the film, closer to the air interface, the films are P3HT-rich and show optical anisotropy in the range of 0–0.5. Films of all three thicknesses show a similar trend as a function of depth throughout the film, and the direction of phase segregation agrees with previous studies for the standard thickness.[12]

The introduction of PCBM into P3HT changes the position of the maximum of $\varepsilon_{2,xy}$ thereby decreasing the anisotropy of the films. This is generally believed to be caused because of torsion and the formation of kinks in the polymer chain.[39] An anisotropy constant of ~0 suggests the presence of amorphous P3HT, whereas an anisotropy constant of >0 suggests crystalline domains.

While the vertical composition profile of the thicker film agrees with previous studies,[12,26,40] as the film thickness is decreased, the BHJ blends become more homogeneous (phase segregation is reduced). As shown in Figure 3, the PCBM (P3HT) percentage found using NEXAFS in the top 5 nm of the films, near the air interface, is found to be 22.9% (77.1%), 24.9% (75.1%), and 41.1% (58.9%) for the 90, 45, and the 15 nm films, respectively. Films of greater thicknesses, ~200 and ~920 nm, were also tested further to confirm the trend of vertical separation as a function of the thickness. The phase segregation for 200 nm-thick films is very similar to that observed in 100 nm-thick films, suggesting an asymptotic limit for film thicknesses ≥100 nm. As the film thicknesses approach the confinement limit (~20 nm), as described by the radius of gyration of the polymer, the polymer crystallites and fullerene aggregates are restricted in their movement and cannot produce a vertical gradient in the P3HT/PCBM volume fraction since the domains completely span the film thickness. A depiction of this mechanism can be seen in Figure 2.

Using SE, we find that the PCBM percentage close to the substrate is 75.1, 62.7, and 47.4% in films with thickness 90, 45, and 15 nm respectively. As shown in Figure 1, these measurements demonstrate a decrease in the vertical separation of the P3HT and PCBM as the thickness of the film decreases. This can be due to a combination of a kinetically limited phenomenon and reduced polymer diffusion due to thin-film confinement.[3]

As previously mentioned, in addition to the EMA model used above, a different model for the BHJ blend was also developed where the electronic transitions are allowed to shift in energy, amplitude, and width compared to the optical constants of pristine P3HT and PCBM films. This model is physically justified by previous studies where the addition of PCBM into P3HT was shown to reduce the degree of order of P3HT within the films.[41] This is believed to be caused by the formation of smaller P3HT domains and the increase in breaks and kinks in the polymer chain caused by the addition of PCBM. Regioregular P3HT can be modeled as a weakly interacting H-aggregate for herringbone and lamellar morphologies.[42] The in-plane imaginary part of the dielectric constant as reconstructed using this model for pure P3HT and the BHJ blend is shown in Figure 4a, along with a schematic of the weakly interacting H-aggregate transitions in Figure 4b.

In order to understand the effect of changing the thickness of the BHJ blend layer on the conjugation length and the optical order of the film, we compare the degree of excitonic coupling within the aggregates. The ratio of the peak heights of the first (0–0) and second (0–1) single exciton state in P3HT is related to W, the free exciton bandwidth, and E_p, the energy of the intramolecular vibrational mode.[42,43] Assuming a Huang–Rhys factor of 1, this relationship is given in eq 7.

$$\frac{A_{0-0}}{A_{0-1}} \approx \left(\frac{1 - \frac{0.24W}{E_p}}{1 + \frac{0.073W}{E_p}} \right)^2 \quad (7)$$

If we assume that a symmetric stretch at 0.18 eV dominates the coupling to the electronic transition,[44] the exciton bandwidth, W can be determined. At a given thickness, we determine W_{EMA} from an EMA model where electronic transitions are not allowed to vary and are fixed to pristine P3HT values and W_{Blend} where the electronic transitions are assumed to be of an independent material and are allowed to vary from the starting values of pristine P3HT. Values for W_{EMA} agree well with literature values for pristine P3HT of ~120 meV, depending on the solvent and concentration.[45] We find W_{EMA} to be 108.6, 146.0, and 121.0 meV for pristine P3HT films spun from solutions of 10, 5, and 2 mg/mL respectively. As expected, there is no

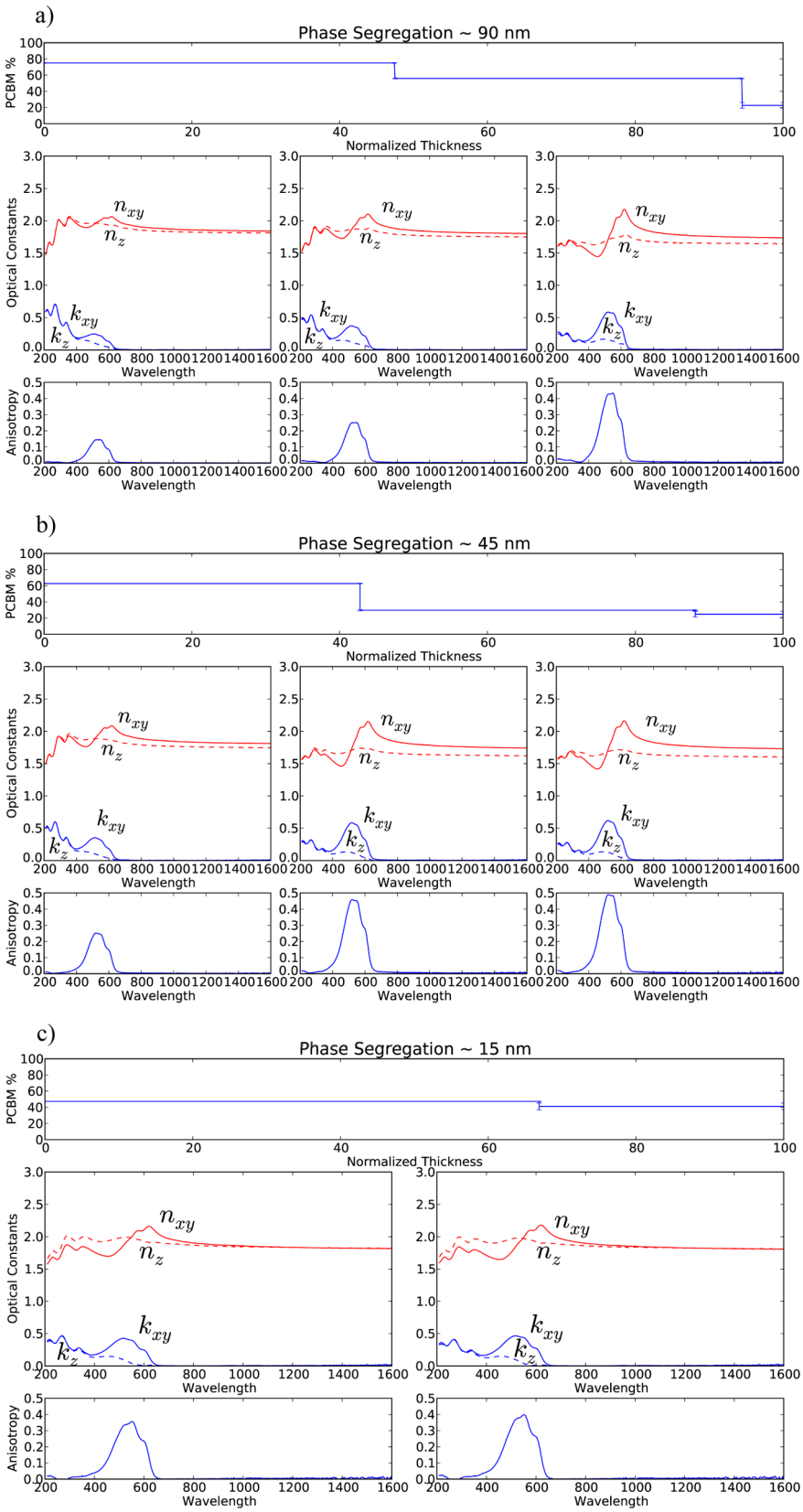

Figure 1. Phase segregation, refractive index, and optical anisotropy in different regions of the film for BHJ films with thicknesses of (a) 90, (b) 45, and (c) 15 nm.

significant change of the exciton bandwidth when the BHJ P3HT transitions are assmued to be the same as that in pristine P3HT. However, we find W_{Blend} to be 255.0, 258.4, and 136.2 meV for 90, 45, and 15 nm,

respectively. The exciton bandwidth significantly increases for a standard-thickness films (>20 nm) after we allow the parameters in the fit to vary. As W increases, the A_1 diminishes with respect to A_2, and the vibronic peaks become irregularly spaced. An increase in W suggests a decrease in the conjugation length and order.[46,47] This decrease can be caused by the addition of PCBM, which causes an increase in breaks and kinks in the P3HT film. The degree of the decrease in conjugation length can be studied by looking at the change in the exciton bandwidth ($\Delta W = W_{Blend} - W_{EMA}$) as a function of the thickness. The shift in the 0−0 and 0−1 energy peaks ($\Delta E_{0-0} = E_{0-0Blend} - E_{0-0EMA}$, $\Delta E_{0-1} = E_{0-1Blend} - E_{0-1EMA}$) also give a sense of the disorder caused by the addition of PCBM. The shifts in energy and in the exciton bandwidth are shown in Figure 5. The error bars represent a 90% confidence interval.

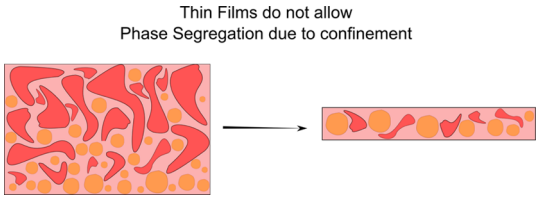

Figure 2. As the thickness of BHJ films is reduced to the confinement limit, the movement of P3HT and PCBM domains is restricted because of their size, and since the domains completely span the film thickness in this limit, no vertical gradient in the P3HT/PCBM volume fraction is observed.

For film thicknesses 45 and 90 nm, the addition of PCBM appears to cause an increase in disorder and a decrease in conjugation length for P3HT, as demonstrated by the large and positive values of ΔW, ΔE_{0-0}, and ΔE_{0-1} for these thicknesses. For the 15 nm thick

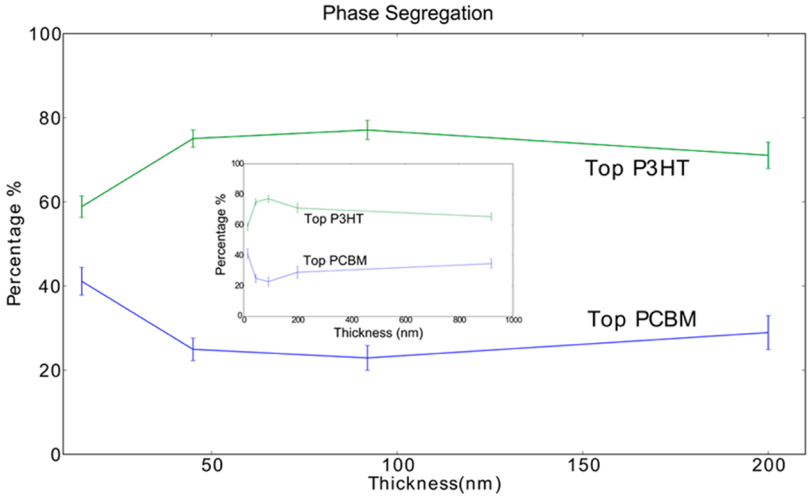

Figure 3. P3HT and PCBM percentages in the top 5 nm section of a film as a function of thickness determined using NEXAFS. Error bars are calculated using the standard deviation of 1000 data sets generated from a bootstrapping technique with replacement. Inset shows P3HT/PCBM percentages as a function of thickness where the thickness varies from 15 to 920 nm.

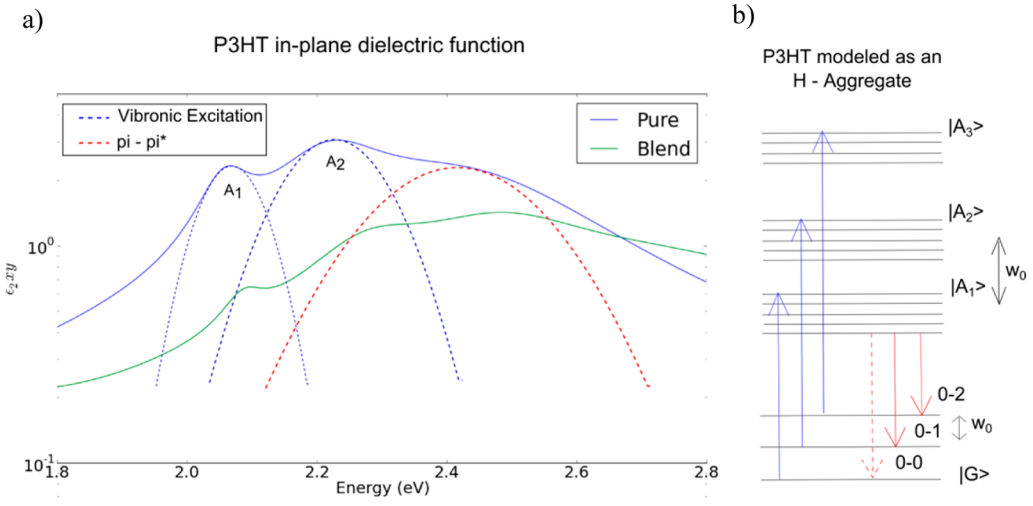

Figure 4. (a) Imaginary part of the dielectric function showing transitions in P3HT, and (b) an energy level diagram for a weakly interacting H-aggregate.

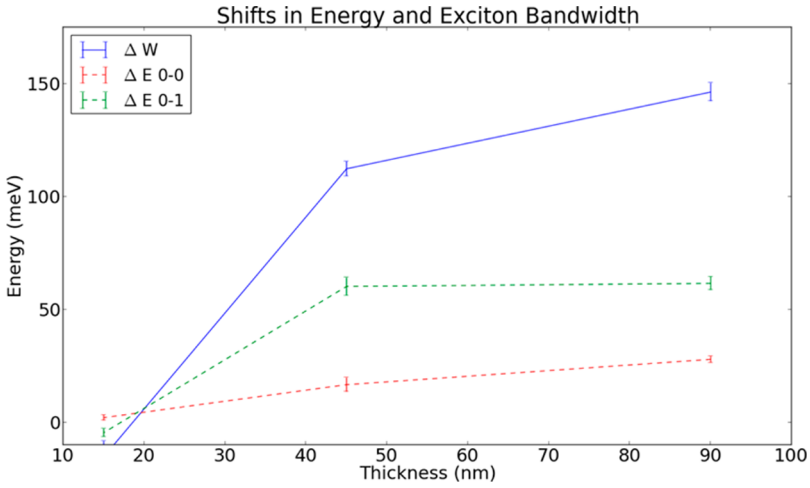

Figure 5. Change in exciton bandwidth (ΔW) and shifts in energy (ΔE 0−0 and ΔE 0−1) shown as a function of thickness.

film, ΔW, ΔE_{0-0}, and ΔE_{0-1} are all near zero, suggesting that the degree of order and conjugation length of P3HT is unafected by the addition of PCBM in these ultrathin films. This may be due to kinetics of film formation (time of drying, *etc.*) or thin-film confinement effects for these ultrathin films.

CONCLUSION

In conclusion, a study of the change in optical anisotropy and the vertical polymer-fullerene composition profile in BHJ blend films at different thicknesses was performed using spectroscopic ellipsometry and NEXAFS. Using a multiple-sample analysis and thickness measurements from different instruments, the anisotropic complex refractive index of blend films was determined. Using this model and NEXAFS studies to find the polymer/fullerene ratio at the interfaces of BHJ films, we determine the vertical polymer-fullerene concentration profile as a function of the thickness of the film. As the film thickness is decreased toward the thin-film confinement regime, the films are found to become less phase segregated. Further it is seen that the degree of disorder and conjugation length of P3HT increase significantly for 45 nm- and 90 nm-thick films, but are unaffected for 15 nm-thick films. This study demonstrates that because of morphological changes, compared to standard-thickness (∼100 nm) films, ultrathin BHJ films (<20 nm) show drastically different optical behavior that must be considered when designing thin-film photovoltaics.

METHODS

Sample Preparation. Poly(3-hexylthiophene) (P3HT) was obtained from Rieke Metal, Inc., (4002-EE, Lot # BS21−21) with a molecular weight, M_w of 40 000−60 000 Da and regioregularity, RR, of 90−94%. [6,6]-Phenyl-C-61-butyric acid methyl ester (PCBM) of purity greater than 99.5% was obtained from American Dye Source, Inc. (ADS61BFA, Lot # 12E011E). The substrates used were microscope slide glass obtained from Thermo Fisher Scientific, and silicon wafers with a native silicon dioxide layer, and also 300 nm silicon dioxide on silicon wafers obtained from Ted Pella, Inc. The substrates were cleaned by sonication for 15 min in acetone, then 15 min in isopropanol, and finally 15 min in deionized water. The cleaned substrates were dried using N_2 gas and exposed to UV ozone for 300 s. P3HT and PCBM solutions were prepared in a 1:1 ratio using 1,2-dichlorobenzene (anhydrous, 99%), Sigma Aldrich, St. Louis, MO. The solutions were prepared inside a glovebox (O_2 < 0.1 ppm, H_2O < 0.1 ppm) and stirred for 2 h at 50 °C using a Teflon coated magnetic stirrer. After stirring they were filtered through a PTFE syringe filter with a pore size of 0.45 μm and transferred into a fresh vial. Total solids solutions were prepared with concentrations of 2, 5, and 10 mg/mL. These were pipetted onto the substrate and spun at 700 rpm for 40 s inside the glovebox. After the films were dry (judging by the drastic visual change in coloration of the film), they were thermally treated at 150 °C for 10 min inside the glovebox. Additionally, pristine P3HT films from concentrations of 2, 5, and 10 mg/mL were prepared using the same process. Pure PCBM films were prepared using a 10 mg/mL solution in anhydrous chloroform (Sigma Aldrich, St. Louis, MO). The PCBM films were spun at 700 rpm for 40 s inside the glovebox and thermally treated on a hot plate at 150 °C for 10 min inside the glovebox.

Variable Angle Spectroscopic Ellipsometry. All measurements were made using a J. A. Woollam V.A.S.E. M-2000 based on the diode array rotating compensator ellipsometer technology. A multiple sample approach was employed where the active material (P3HT:PCBM) was spun on three different substrates using the same processing conditions,[27] including (1) microscope slide glass, (2) silicon with a native oxide, and (3) silicon with a thermal oxide (300 nm) layer. It was assumed that the optical properties of the active layers on all three substrates were identical and that any changes in the spectra were due to the substrate. This method results in multiple sets of unique data for the same system allowing for greater confidence that the fits to a parametrized model are causal and not correlated. Ellipsometric measurements were first made on the cleaned bare substrates. All data were taken in the wavelength range of 210 to 1700 nm at angles of 45 to 75 degrees in divisions of 7.5 degrees. The built-in autoalignment function of the M-2000 was used to align the sample before the measurement. For each sample, a second measurement was taken at a different spot on the film to reduce random error. The data collected from the three substrates were analyzed simultaneously to yield solutions for the complex refractive index and the film thickness. The ellipsometric data were analyzed by simultaneously fitting identical models for the active layer on each substrate that were

defined with coupled complex refractive indices of the active layers using the WVASE32 software (version 3.770, J. A. Woollam Co.). The best fit for the optical constants was found by minimizing the mean square error (MSE) between the measured and the modeled curves using the Levenberg–Marquardt multivariate regressions algorithm. The complex refractive indices from the SE modeling were confirmed by making UV–vis–IR transmission/reflection measurements using a Perkin-Elmer Lamda 950 UV–vis–NIR spectrophotometer and modeling the data (using FDTD from Lumerical Solutions, Inc.) with the SE-measured complex refractive indices as input. Thickness results from ellipsometry were confirmed using stylus profilometry (Tencor Instruments, AlphaStep 200) and atomic force microscopy in tapping mode using the film scratch method[48] (AFM, Asylum Research Model MFP-3D).

SE data consists of direct measurement of the complex ratio of the reflection amplitudes of polarized light with electric field within (r_p) and perpendicular (r_s) to the plane of incidence as a function of the angle of incidence.[29,36] From this data, plots of ψ and Δ *versus* angle of incidence are determined from the definition of ψ and Δ in eq 8.

$$\frac{r_p}{r_s} = \tan(\psi)e^{i\Delta} \quad (8)$$

The angle of incidence in the measurement is varied between 45 and 75 degrees in increments of 7.5 degrees. This range includes the Brewster angle at which the sensitivity of the measurement is highest. The large range is used so that parameter correlation can be reduced in the fitting process and sensitivity to morphology, anisotropy and composition changes can be enhanced. The measurement was done at room temperature (~25 °C) and in air.

Near Edge X-ray Absorption Fine-Structure Spectroscopy (NEXAFS). NEXAFS spectroscopy was performed at the National Institute of Standards and Technology facility (beamline U7A) at the National Synchrotron Light Source (NSLS) of Brookhaven National Laboratory for soft X-ray materials characterization. Data were collected in the energy range of 270 to 320 eV around the carbon K-edge (at 285 eV) in partial electron yield (PEY) mode with a grid bias of 50 V.

Spectra from pure P3HT and PCBM films were extracted individually. A linear combination of these spectra were then used to fit the spectra obtained from the blend films, thus yielding the P3HT and PCBM volume fractions in the top 5 nm of the film.

Conflict of Interest: The authors declare no competing financial interest.

Acknowledgment. Research was carried out in part at the Center for Functional Nanomaterials, Brookhaven National Laboratory, which is supported by the U.S. Department of Energy, Office of Basic Energy Sciences, under Contract No. DE-AC02-98CH10886. Use of the National Synchrotron Light Source, Brookhaven National Laboratory, was supported by the U.S. Department of Energy, Office of Science, Office of Basic Energy Sciences, under Contract No. DE-AC02-98CH10886. This work was also partially supported by the U.S. Department of Energy, Sustainable Energy Technologies Department (A.A., D.M.N.M.D., and M.D.E.) under Contract DE-AC02-98CH10886, the Materials Sciences and Engineering Division (D.G.) under Contract DE-AC02-98CH10886, and was partially supported by the Laboratory Research and Development Initiative at Brookhaven National Laboratory.

Supporting Information Available: Device fabrication, the measurement process for variable angle spectroscopic ellipsometry (VASE), the fitting procedure, including the maximum likelihood estimator and determination of an accurate VASE model using a Monte Carlo technique, and normalized spectra from near edge X-ray absorption fine structure spectroscopy. This material is available free of charge *via* the Internet at http://pubs.acs.org.

REFERENCES AND NOTES

1. Indrakanti, A.; Jones, R. L.; Kumar, S. K. Do "Nonequilibrium" Effects Control Strong Surface Segregation from Polymer Blends? *Macromolecules* **2004**, *37*, 9–12.
2. Jones, R. L.; Indrakanti, A.; Briber, R. M.; Muller, M.; Kumar, S. K. Phase Behavior of Ultrathin Polymer Mixtures. *Macromolecules* **2004**, *37*, 6676–6679.
3. Soles, C. L.; Douglas, J. F.; Wu, W.; Dimeo, R. M. Incoherent Neutron Scattering as a Probe of the Dynamics in Molecularly Thin Polymer Films. *Macromolecules* **2003**, *36*, 373–379.
4. Soles, C. L.; Lin, E. K.; Lenhart, J. L.; Jones, J. L.; Wu, W.; Goldfarb, D. L.; Angelopoulos, M. Thin Film Confinement Effects on the Thermal Properties of Model Photoresist Polymers. *J. Vac. Sci. Technol., B: Microelectron. Nanometer Struct.--Process., Meas., Phenom.* **2001**, *19*, 2690.
5. Goldfarb, D. L.; Angelopoulos, M.; Lin, E. K.; Jones, R. L.; Soles, C. L.; Lenhart, J. L.; Wu, W. Confinement Effects on the Spatial Extent of the Reaction Front in Ultrathin Chemically Amplified Photoresists. *J. Vac. Sci. Technol., B: Microelectron. Nanometer Struct.--Process., Meas., Phenom.* **2001**, *19*, 2699.
6. Chiu, M.; Jeng, U.; Su, C.; Liang, K. S.; Wei, K. Simultaneous Use of Small- and Wide-Angle X-ray Techniques to Analyze Nanometerscale Phase Separation in Polymer Heterojunction Solar Cells. *Adv. Mater.* **2008**, *20*, 2573–2578.
7. Allen, J. E.; Yager, K. G.; Hlaing, H.; Nam, C.; Ocko, B. M.; Black, C. T. Enhanced Charge Collection in Confined Bulk Heterojunction Organic Solar Cells. *Appl. Phys. Lett.* **2011**, *99*, 163301.
8. Li, G.; Shrotriya, V.; Huang, J.; Yao, Y.; Moriarty, T.; Emery, K.; Yang, Y. High-Efficiency Solution Processable Polymer Photovoltaic Cells by Self-Organization of Polymer Blends. *Nat. Mater.* **2005**, *4*, 864–868.
9. Chen, W.; Nikiforov, M. P.; Darling, S. B. Morphology Characterization in Organic and Hybrid Solar Cells. *Energy Environ. Sci.* **2012**, *5*, 8045.
10. Stalder, R.; Grand, C.; Subbiah, J.; So, F.; Reynolds, J. R. An Isoindigo and Dithieno[3,2-b:2′,3′-d]Silole Copolymer for Polymer Solar Cells. *Polym. Chem.* **2011**, *3*, 89.
11. Arias, A. C.; Corcoran, N.; Banach, M.; Friend, R. H.; MacKenzie, J. D.; Huck, W. T. S. Vertically Segregated Polymer-Blend Photovoltaic Thin-Film Structures Through Surface-Mediated Solution Processing. *Appl. Phys. Lett.* **2002**, *80*, 1695.
12. Germack, D. S.; Chan, C. K.; Kline, R. J.; Fischer, D. A.; Gundlach, D. J.; Toney, M. F.; Richter, L. J.; DeLongchamp, D. M. Interfacial Segregation in Polymer/Fullerene Blend Films for Photovoltaic Devices. *Macromolecules* **2010**, *43*, 3828–3836.
13. Beiley, Z.; Bowring, A.; McGehee, M. D. *Modeling Low-Cost Hybrid Tandem Photovoltaics with Power Conversion Efficiencies Exceeding 20%*; Institute of Electrical and Electronics Engineers: New York, 2012; pp 003129–003130.
14. Mayer, A.; Scully, S.; Hardin, B.; Rowell, M.; McGehee, M. D. Polymer-Based Solar Cells. *Mater. Today* **2007**, *10*, 28–33.
15. Pang, Y.; Dissanayake, N.; Eisaman, M. D. *Guided-Mode Absorption in Ultrathin Organic Photovoltaics*; Institute of Electrical and Electronics Engineers: New York, 2012; pp 003131–003136.
16. Callahan, D. M.; Munday, J. N.; Atwater, H. A. Solar Cell Light Trapping Beyond the Ray Optic Limit. *Nano Lett.* **2012**, *12* (1), 214–218.
17. Ferry, V. E.; Verschuuren, M. A.; Li, H. B. T.; Verhagen, E.; Walters, R. J.; Schropp, R. E. I.; Atwater, H. A.; Polman, A. Light Trapping in Ultrathin Plasmonic Solar Cells. *Opt. Express* **2010**, *18*, A237.
18. Green, M. A. Enhanced Evanescent Mode Light Trapping in Organic Solar Cells and Other Low Index Optoelectronic Devices. *Prog. Photovoltaics* **2011**, *19*, 473–477.
19. Norwood, R.; Gangopadhay, P.; Shahin, S. Ultra-thin Organic Photovoltaics with Increased Efficiency. *SPIE Newsroom* **2012**, 10.1117/2.1201212.004593.
20. Saeta, P. N.; Ferry, V. E.; Pacifici, D.; Munday, J. N.; Atwater, H. A. How Much Can Guided Modes Enhance Absorption in Thin Solar Cells? *Opt. Express* **2009**, *17*, 20975.
21. Shahin, S.; Gangopadhyay, P.; Norwood, R. A. Ultrathin Organic Bulk Heterojunction Solar Cells: Plasmon Enhanced Performance Using Au Nanoparticles. *Appl. Phys. Lett.* **2012**, *101*, 053109.

22. Yu, Z.; Raman, A.; Fan, S. Fundamental Limit of Nanophotonic Light Trapping in Solar Cells. *Proc. Natl. Acad. Sci.* **2010**, *107*, 17491–17496.
23. Collins, B. A.; Li, Z.; Tumbleston, J. R.; Gann, E.; McNeill, C. R.; Ade, H. Absolute Measurement of Domain Composition and Nanoscale Size Distribution Explains Performance in PTB7:PC71BM Solar Cells. *Adv. Energy Mater.* **2013**, *3*, 65–74.
24. Huang, J.; Yao, Y.; Moriarty, T.; Emery, K.; Li, G.; Shrotriya, V.; Yang, Y. High-Efficiency Solution Processable Polymer Photovoltaic Cells by Self-Organization of Polymer Blends. *Nat. Mater.* **2005**, *4*, 864–868.
25. Campoy-Quiles, M.; Nelson, J.; Etchegoin, P. G.; Bradley, D. D. C.; Zhokhavets, V.; Gobsch, G.; Vaughan, H.; Monkman, A.; Ingänas, O.; Persson, N. K.; *et al.* On the Determination of Anisotropy in Polymer Thin Films: A Comparative Study of Optical Techniques. *Phys. Status Solidi (C)* **2008**, *5*, 1270–1273.
26. Karagiannidis, P. G.; Georgiou, D.; Pitsalidis, C.; Laskarakis, A.; Logothetidis, S. Evolution of Vertical Phase Separation in P3HT:PCBM Thin Films Induced by Thermal Annealing. *Mater. Chem. Phys.* **2011**, *129*, 1207–1213.
27. Järrendahl, K.; Arwin, H. Multiple Sample Analysis of Spectroscopic Ellipsometry Data of Semi-Transparent Films. *Thin Solid Films* **1998**, *313−314*, 114–118.
28. Zhokhavets, U.; Erb, T.; Gobsch, G.; Al-Ibrahim, M.; Ambacher, O. Relation Between Absorption and Crystallinity of Poly(3-hexylthiophene)/Fullerene Films for Plastic Solar Cells. *Chem. Phys. Lett.* **2006**, *418*, 347–350.
29. Fujiwara, H. *Spectroscopic Ellipsometry: Principles and Applications*; Wiley: New York, 2007.
30. Engmann, S.; Turkovic, V.; Denner, P.; Hoppe, H.; Gobsch, G. Optical Order of the Polymer Phase within Polymer/Fullerene Blend Films. *J. Polym. Sci. B: Polym. Phys.* **2012**, *50*, 1363–1373.
31. Bertolucci, M. D.; Harris, D. C. *Symmetry and Spectroscopy: An Introduction to Vibrational and Electronic Spectroscopy*; Courier Dover Publications: Mineola, NY, 1978.
32. Jellison, G. E.; Modine, F. A. Parameterization of the Optical Functions of Amorphous Materials in the Interband Region. *Appl. Phys. Lett.* **1996**, *69*, 371.
33. Kelly, M.; Etchegoin, P.; Fuchs, D.; Krätschmer, W.; Fostiropoulos, K. Optical Transitions of C60 Films in the Visible and Ultraviolet from Spectroscopic Ellipsometry. *Phys. Rev. B* **1992**, *46*, 4963–4968.
34. Richter, W.; McGilp, J. F. Optical *in-situ* Surface Control During Moype and MBE Growth [and Discussion]. *Philos. Trans. R. Soc., A* **1993**, *344*, 453–467.
35. Bruggeman, D. A. G. Berechnung Verschiedener Physikalischer Konstanten Von Heterogenen Substanzen. I. Dielektrizitätskonstanten Und Leitfähigkeiten der Mischkörper aus Isotropen Substanzen. *Annalen der Physik* **1935**, *416*, 636–664.
36. Tompkins, H.; Irene, E. A. *Handbook of Ellipsometry (Materials Science and Process Technology)*; William Andrew: Norwich, NY, 2006.
37. Kiel, J. W.; Kirby, B. J.; Majkrzak, C. F.; Maranville, B. B.; Mackay, M. E. Nanoparticle Concentration Profile in Polymer-Based Solar Cells. *Soft Matter* **2010**, *6*, 641.
38. Orimo, A.; Masuda, K.; Honda, S.; Benten, H.; Ito, S.; Ohkita, H.; Tsuji, H. Surface Segregation at the Aluminum Interface of Poly(3-hexylthiophene)/Fullerene Solar Cells. *Appl. Phys. Lett.* **2010**, *96*, 043305.
39. Beenken, W. J. D.; Pullerits, T. Spectroscopic Units in Conjugated Polymers: A Quantum Chemically Founded Concept? *J. Phys. Chem. B* **2004**, *108*, 6164–6169.
40. Campoy-Quiles, M.; Ferenczi, T.; Agostinelli, T.; Etchegoin, P. G.; Kim, Y.; Anthopoulos, T. D.; Stavrinou, P. N.; Bradley, D. D. C.; Nelson, J. Morphology Evolution *via* Self-Organization and Lateral and Vertical Diffusion in Polymer:Fullerene Solar Cell Blends. *Nat. Mater.* **2008**, *7*, 158–164.
41. Lilliu, S.; Agostinelli, T.; Pires, E.; Hampton, M.; Nelson, J.; Macdonald, J. E. Dynamics of Crystallization and Disorder During Annealing of P3HT/PCBM Bulk Heterojunctions. *Macromolecules* **2011**, *44*, 2725–2734.
42. Spano, F. C. Modeling Disorder in Polymer Aggregates: The Optical Spectroscopy of Regioregular Poly(3-hexylthiophene) Thin Films. *J. Chem. Phys.* **2005**, *122*, 234701.
43. Clark, J.; Silva, C.; Friend, R.; Spano, F. Role of Intermolecular Coupling in the Photophysics of Disordered Organic Semiconductors: Aggregate Emission in Regioregular Polythiophene. *Phys. Rev. Lett.* **2007**, *98*, 20.
44. Louarn, G.; Trznadel, M.; Buisson, J. P.; Laska, J.; Pron, A.; Lapkowski, M.; Lefrant, S. Raman Spectroscopic Studies of Regioregular Poly(3-alkylthiophenes). *J. Phys. Chem.* **1996**, *100*, 12532–12539.
45. Clark, J.; Chang, J.; Spano, F. C.; Friend, R. H.; Silva, C. Determining Exciton Bandwidth and Film Microstructure in Polythiophene Films Using Linear Absorption Spectroscopy. *Appl. Phys. Lett.* **2009**, *94*, 163306.
46. Beljonne, D.; Cornil, J.; Silbey, R.; Millié, P.; Brédas, J. L. Interchain Interactions in Conjugated Materials: The Exciton Model *Versus* the Supermolecular Approach. *J. Chem. Phys.* **2000**, *112*, 4749.
47. Manas, E. S.; Spano, F. C. Absorption and Spontaneous Emission in Aggregates of Conjugated Polymers. *J. Chem. Phys.* **1998**, *109*, 8087.
48. Meyer, E. Atomic Force Microscopy. *Prog. Surf. Sci.* **1992**, *41*, 3–49.